Non-covalent DNA binding and cytotoxicity of certain mixed-ligand ruthenium(II) complexes of 2,2′-dipyridylamine and diimines†

Venugopal Rajendiran,[a] Mariappan Murali,‡[a] Eringathodi Suresh,[b] Mallayan Palaniandavar,*[a] Vaiyapuri Subbarayan Periasamy[c] and Mohammad Abdulkader Akbarsha[c]

Received 1st October 2007, Accepted 30th January 2008
First published as an Advance Article on the web 6th March 2008
DOI: 10.1039/b715077f

A series of mixed ligand ruthenium(II) complexes $[Ru(Hdpa)_2(diimine)](ClO_4)_2$ **1–5**, where Hdpa is 2,2′-dipyridylamine and diimine is 1,10-phenanthroline (phen) and a modified/extended 1,10-phenanthroline such as, 5,6-dimethyl-1,10-phenanthroline (5,6-dmp), dipyrido[3,2-*d*:2′,3′-*f*]quinoxaline (dpq), 5-methyldipyrido[3,2-*d*:2′,3′-*f*]quinoxaline (mdpq) and dipyrido[3,2-*a*:2′,3′-*c*]phenazine (dppz) have been isolated and characterized by analytical and spectral methods. The complex $[Ru(Hdpa)_2(phen)](PF_6)_2$ **1** has been structurally characterized and the coordination geometry around Ru(II) in it is described as distorted octahedral. ^{1}H NMR spectral data reveal that **1–5** should have a C_2 symmetry lying on the diimine plane due to the rapid flapping of the coordinated Hdpa ligands. The interaction of the complexes with calf thymus (CT) DNA has been explored by using absorption and emission spectral and viscometry and electrochemical techniques and the mode of DNA binding of the complexes has been proposed. The DNA binding affinity of the complexes decreases with decrease in number of planar aromatic rings in the co-ligand supporting the intercalation of the diimine co-ligands in between the DNA base pairs. Circular dichroic spectral studies reveal that the complexes **3–5** exhibit induced circular dichroism upon binding to CT DNA. Interestingly, upon interaction with CT DNA all the complexes show an increase in anodic current in the cyclic voltammograms suggesting that they are involved in electrocatalytic guanine oxidation. Interestingly, of all the complexes, only **5** alters the DNA superhelicity upon binding with supercoiled pBR322 DNA, which is consistent with its higher DNA binding affinity. Further, the cytotoxicities of the complexes against human cervical epidermoid carcinoma cell line (ME180) have been examined. Interestingly, **5** exhibits a cytotoxicity against ME180 higher than other complexes with potency approximately 8 times more than cisplatin for 24 h incubation but 4 times lower than cisplatin for 48 h incubation.

Introduction

The designing of non-covalent DNA binding ruthenium(II) anticancer drugs is growing in interest in the field of metallopharmaceuticals[1] because the covalently DNA binding anticancer agent cisplatin possesses inherent limitations such as high toxicity and low administration dosage.[2] The mechanism of action of DNA-targeting metal-based drugs has been thought to involve covalent binding to nucleobase moieties and a low degree of selectivity.[3] So, there is considerable attention focused on the design of new metal-based drugs that exhibit enhanced selectivity and novel modes of DNA interaction such as non-covalent interactions that mimic the mode of interaction of proteins with DNA.[4] Very recently non-covalent DNA binding metal complexes,[1] particularly, metallointercalators have received attention in designing efficient anticancer drugs.[5] Intercalation, which is well-known to strongly influence the properties of DNA, has been reported as a preliminary step in mutagenesis.[6] Non-covalent interactions between transition-metal complexes and DNA occur by intercalation, groove binding, or electrostatic surface binding. In particular, metal complexes possessing planar aromatic ligands, which bind to DNA by intercalation, is receiving considerable attention.[7] Such metallointercalators tend to be strongly mutagenic and some have shown promising chemotherapeutic activity, which correlates well with their DNA binding affinity.[8] Also, complexes that contain the appropriately orientated H-bonding functionalities permit effective binding to DNA either in the major or minor grooves.[9]

Ruthenium complexes are regarded as promising alternatives to platinum complexes and several ruthenium complexes have been now proposed as potential anticancer substances,[10] demonstrating remarkable anticancer activity and showing general toxicity lower than platinum compounds.[11] Thus the Ru(III) complex ImH[*trans*-$RuCl_4$(DMSO)(Im)], NAMI-A, shows high selectivity for solid tumor metastases[12] (prevents spread of cancer) and low host

[a]*School of Chemistry, Bharathidasan University, Tiruchirappalli, 620 024, Tamilnadu, India. E-mail: palanim51@yahoo.com*
[b]*Analytical Science Discipline, Central Salt and Marine Chemical Research Institute, Bhavnagar, 364 002, India*
[c]*Department of Animal Science, Bharathidasan University, Tiruchirapalli, 620 024, India*

† Electronic supplementary information (ESI) available: ^{1}H NMR spectral data for ligands and Figs. S1 and S2. CCDC reference numbers 660567–660570. For crystallographic data in CIF or other electronic format see DOI: 10.1039/b715077f

‡ Present Address: Department of Chemistry, National College, Tiruchirappalli 620 001, Tamil Nadu, India.

toxicity[13] and is the first ruthenium complex to enter clinical trials.[13b] However, it fails to affect primary tumor growth[14] and does not exhibit cytotoxicity against tumor cells *in vitro*. A related Ru(III) compound,[15] KP1019, has also entered clinical trials, as it was found to exhibit antiproliferative activity *in vitro* in human colon carcinoma cell lines.[16] Very recently, Sadler and his co-workers have reported half-sandwich Ru(II) arene complexes, which exhibit reproducible anticancer activity against A2780 human ovarian cancer cell lines both *in vitro* and *in vivo*.[17] Since DNA has been identified as the possible primary molecular target[18] of metal-based anticancer agents such as cisplatin,[2a] attention is mainly focused on interacting ruthenium complexes with DNA to identify whether DNA binding is effective and whether they can act as chemotherapeutic agents. These ruthenium(III) complexes are considered as prodrugs because the activity seems to be initiated by reduction of Ru(III) to Ru(II) once the core complex is inside the anoxic cancer tissues, followed by linkage to nucleic acids. Therefore, in the field of biocoordination Chemistry development of Ru(II) anticancer complexes that have both appreciable solubility in aqueous media and uptake by the cells have received much attention because the reduction step is skipped.[19] In our earlier study we have shown[8] that the non-covalently DNA binding complex $[Ru^{II}(N_2S_2)(dppz)]^{2+}$ exhibits a significant cytotoxicity against melanoma cancer cell line (A375).

In this report we explore the DNA binding properties of a series of ruthenium(II) complexes of the type $[Ru(Hdpa)_2(diimine)]^{2+}$ **1–5**, where Hdpa is 2,2′-dipyridylamine and diimine is a modified/extended aromatic 1,10-phenanthroline (Scheme 1) such as 1,10-phenanthroline (phen) (**1**), 5,6-dimethyl-1,10-phenanthroline (5,6-dmp) (**2**), dipyrido[3,2-*d*:2′,3′-*f*]quinoxaline (dpq) (**3**), 5-methyldipyrido[3,2-*d*:2′,3′-*f*]quinoxaline (5-mdpq) (**4**) and dipyrido[3,2-*a*:2′,3′-*c*]phenazine (dppz) (**5**). The rationale behind the design of the complexes is that the bidentate primary ligand Hdpa offers flexibility around the secondary amine nitrogen bridging the two pyridine rings, the two pyridine planes adopting either coplanar or tilted conformation upon coordination to metal centers.[20] Also, Hdpa possesses the potential to form hydrogen bond with suitable DNA functionalities, which would be expected to enhance the DNA binding affinity significantly. The co-ligands phen and extended 1,10-phenanthrolines with different numbers of aromatic rings to vary the surface area for intercalation would be expected to act as affinity ligands, and dictate the extent of DNA binding interaction of the complexes. The complexes are coordinatively saturated and rigid and so no covalent DNA binding is expected. The phen complex **1** has been structurally characterized. The DNA binding of the Ru(II) complexes has been studied by using a variety of physical methods such as absorption and emission spectroscopy, viscosity and electrochemical techniques. The ability of the complexes to unwind/untwist DNA has been studied by using supercoiled pBR322 DNA. The cytotoxicity of the complexes **1–5** has been studied by screening the complexes against human epidermoid carcinoma (ME180) cell line. It is remarkable that the complex **5** exhibits a cytotoxicity higher than the other complexes. Also, it displays cytotoxicity in the range of cisplatin, which is in clinical use currently.

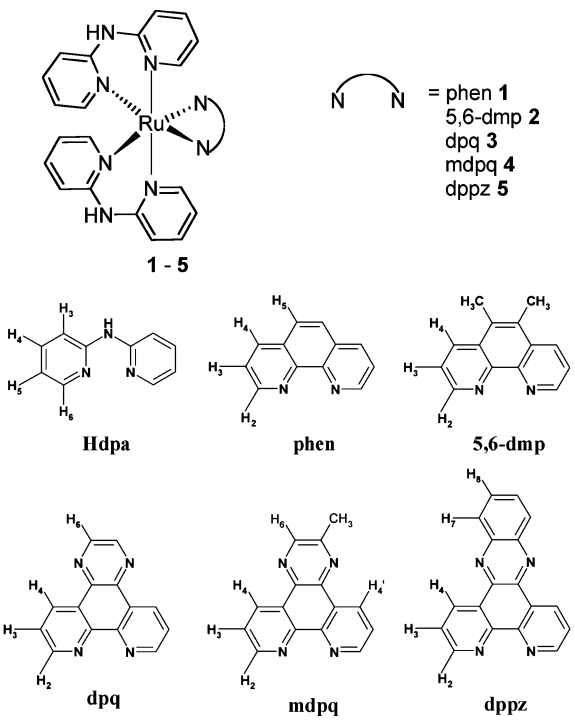

Scheme 1 Possible coordination geometries of mixed ligand ruthenium(II) complexes of Hdpa and structures of diimine (N–N) co-ligands and proton numbering pattern.

Experimental

Reagents and materials

$RuCl_3 \cdot 3H_2O$ (Arora Matthey), 1,10-phenanthroline (Merck), 2,2′-dipyridylamine (Aldrich), calf thymus (CT) DNA (highly polymerized stored at 4 °C), Hoechst 33258 (Sigma), the self-complementary oligonucleotides d(GCGCGCGCGCGC) referred as $d(GC)_{12}$, d(ATATATATATAT) referred as $d(AT)_{12}$ and d(CGCGATCGCG) referred as $d(CGCGATCGCG)_2$ were purchased from Sigma and stored at −20 °C. The lyophilized oligonucleotides were digested in Tris buffer and annealed using standard procedures to make the double-stranded oligonucleotides and stored at 4 °C. The concentrations of the oligonucleotide solutions were determined using the procedures provided by the supplier and pBR322 supercoiled plasmid DNA (stored at −20 °C) and agarose (Genei) and cisplatin (Bristol-Myers Squibb Co., Princeton) were used as received. Ultra-pure Milli-Q water (18.2 mΩ) was used in all experiments. Reagent grade solvents were dried and distilled by usual methods and the solvents were stored over molecular sieves (4 Å).

Methods and instrumentation

Microanalysis (C, H and N) were carried out with Vario EL elemental analyzer. An LCQ DECA XP electrospray mass spectrometer was employed for ESI-MS analysis. UV-Vis spectroscopy was recorded on a Varian Cary 300 Bio UV-Vis spectrophotometer using cuvettes of 1 cm path length. Emission intensity measurements were carried out using Jasco F 6500 spectrofluorometer. Circular dichroic spectra of DNA were obtained by using JASCO J-716 spectropolarimeter equipped with a Peltier temperature

control device. Viscosity measurements were carried out using Schott Gerate AVS 310 automated viscometer.

Solutions of DNA in the buffer 50 mM NaCl–5 mM Tris HCl in water gave the ratio of UV absorbance at 260 and 280 nm, A_{260}/A_{280}, as 1.9[21] indicating that the DNA was sufficiently free of protein. Concentrated stock solutions of DNA (13.5 mM) were prepared in buffer and sonicated for 25 cycles, where each cycle consisted of 30 s with 1 min intervals. The concentration of DNA in nucleotide phosphate (NP) was determined by UV absorbance at 260 nm after 1 : 100 dilutions. The extinction coefficient, ε_{260}, was taken as 6600 M^{-1} cm^{-1}. Stock solutions were stored at 4 °C and used after no more than 4 days. Supercoiled plasmid pBR322 DNA was stored at −20 °C and the concentration of DNA in base pairs was determined by UV absorbance at 260 nm after appropriate dilutions taking ε_{260} as 13 100 M^{-1} cm^{-1}. Concentrated stock solutions of metal complexes were prepared by dissolving calculated amounts of metal complexes in respective amount of solvent and diluted suitably with corresponding buffer to required concentrations for all the experiments.

Synthesis of ligands

The ligands dipyrido[3,2-*d*:2′,3′-*f*]quinoxaline (dpq),[22] 5-methyldipyrido[3,2-*d*:2′,3′-*f*]quinoxaline (mdpq)[22] and dipyrido[3,2-*a*:2′,3′-*c*]phenazine (dppz)[23] were synthesised according to literature methods.

Synthesis of Ru(II) complexes

CAUTION

During handling of the perchlorate salts of metal complexes with organic ligands care should be taken because of the possibility of explosion.

Synthesis of *cis*-[Ru(Hdpa)$_2$(Cl$_2$)]Cl·H$_2$O. A mixture of $RuCl_3 \cdot 3H_2O$ (0.52 g, 2 mmol) and Hdpa (4.2 mmol, 0.71 g) was refluxed in 80 mL of ethanol for 8 h, and filtered. The filtrate was concentrated to about 40 ml and a green product was obtained after stored in a refrigerator for overnight.

Synthesis of [Ru(Hdpa)$_2$(phen)](ClO$_4$)$_2$ 1. A mixture of *cis*-[Ru(Hdpa)$_2$(Cl$_2$)]Cl (0.15 g, 0.26 mmol) and phen (0.0515 g, 0.26 mmol) was heated to reflux in water (30 mL) for 15 min under N_2 atmosphere, after which the solution was cooled then the reducing agent 30% H_3PO_3 neutralized with NaOH was added to the reaction mixture and the reflux were continued to 3 h and treated with an excess of $NaClO_4$. The precipitated complex was dried, dissolved in a small amount of acetonitrile, and purified by chromatography over alumina using acetonitrile–methanol (3 : 1, v/v) as an eluent. The red coloured compound was obtained after drying in *vacuo*. Yield, 0.16 g, 73%. Red coloured single crystals of **1**, suitable for X-ray studies were obtained on slow evaporation of the complex in an acetonitrile–*n*-butanol (1 : 3) mixture. Anal. Calc. for $RuC_{32}H_{26}N_8Cl_2O_8$: C, 46.73; H, 3.19; N, 13.62. Found: C, 46.30; H, 3.20; N, 13.43%. λ_{max}/nm (ε/M^{-1} cm^{-1}) (5% CH_3OH–5 mM Tris-HCl–50 mM NaCl buffer (0.5 : 9.5, v/v) buffer at pH 7.1): 505 (sh), 451 (6582), 423 (sh) (7113), 380 (7895), 283 (45 211), 265 (61 386), 230 (41 147). ESI-MS: $[Ru(Hdpa)_2(phen)]^{2+}$ displays a peak at m/z = 312.0, calc. 311.8. ^{1}H NMR (DMSO-d_6, 400 MHz): δ (multiplicity, integration, assignment, J/Hz, coordination-induced shifts (c.i.s.), $\delta_{complex} - \delta_{ligand}$)/ppm. Group I, 8.734 (d, 2H, H_2, 8.1, −0.514), 8.042 (t, 2H, H_3, 4.1, 0.178), 9.173 (d, 2H, H_4, 5.2, 0.603), 8.258 (s, 2H, H_5, 0.210). Group II, 7.410 (d, 2H, H_3, 8.3, −0.327), 7.986 (t, 2H, H_4, 4.4, 0.350), 6.983 (t, 2H, H_5, 6.5, 0.136), 7.762 (d, 2H, H_6, 4.8, −0.451). Group III, 7.007 (d, 2H, H_3, 8.3, −0.730), 7.528 (t, 2H, H_4, 4.3, −0.108), 6.485 (t, 2H, H_5, 6.5, −0.362), 7.118 (d, 2H, H_6, 4.4, −1.095) and 10.699 (s, 2H, NH, 1.067).

Synthesis of [Ru(Hdpa)$_2$(5,6-dmp)](ClO$_4$)$_2$ 2. This was prepared by refluxing *cis*-[Ru(Hdpa)$_2$(Cl$_2$)]Cl (0.15 g, 0.26 mmol) and 5,6-dmp (0.054 g, 0.26 mmol) using the procedure employed for **1**. Yield: 0.18 g (81%). Anal. Calc. for $RuC_{34}H_{30}N_8Cl_2O_8$: C, 48.01; H, 3.55; N, 13.17. Found: C, 48.00; H, 3.42; N, 13.13%. λ_{max}/nm (ε/M^{-1} cm^{-1}) (5% CH_3OH–5 mM Tris-HCl–50 mM NaCl buffer (0.5 : 9.5, v/v) buffer at pH 7.1): 505 (sh), 453 (5673), 423 (sh) (6067), 389 (6497), 290 (31 864), 272 (51 434), 240 (33 736). ESI-MS: $[Ru(Hdpa)_2(5,6\text{-dmp})]^{2+}$ displays a peak at m/z = 325.6, calc. 325.8. ^{1}H NMR (DMSO-d_6, 400 MHz): δ (multiplicity, integration, assignment, J/Hz, c.i.s.)/ppm. Group I, 8.829 (d, 2H, H_2, 8.1, −0.262), 8.031 (t, 2H, H_3, 4.2, 0.474), 9.089 (d, 2H, H_4, 5.1, 0.784), 2.781 (s, 6H, CH_3, 0.207). Group II, 7.374 (d, 2H, H_3, 8.2, −0.363), 7.988 (t, 2H, H_4, 7.9, 0.352), 6.985 (t, 2H, H_5, 6.2, 0.138), 7.740 (d, 2H, H_6, 4.8, −0.473). Group III, 6.991 (d, 2H, H_3, 7.5, −0.746), 7.531 (t, 2H, H_4, 7.4, −0.105), 6.479 (t, 2H, H_5, 6.2, −0.368), 7.044 (d, 2H, H_6, 4.9, −1.169) and 10.653 (s, 2H, NH, 1.021).

Synthesis of [Ru(Hdpa)$_2$(dpq)](ClO$_4$)$_2$ 3. This was prepared by refluxing *cis*-[Ru(Hdpa)$_2$(Cl$_2$)]Cl (0.2 g, 0.35 mmol) and dpq (0.060 g, 0.35 mmol) using the procedure employed for **1**. Yield: 0.26 g (88%). Anal. Calc. for $RuC_{34}H_{26}N_8Cl_2O_8$: C, 46.69; H, 3.00; N, 16.02. Found: C, 46.20; H, 2.95; N, 15.96%. λ_{max}/nm (ε/M^{-1} cm^{-1}) (5% CH_3OH–5 mM Tris-HCl–50 mM NaCl buffer (0.5 : 9.5, v/v) buffer at pH 7.1): 522 (sh), 466 (5225), 434 (sh) (5367), 284 (46 952), 269 (6359), 257 (55 008). ESI-MS: $[Ru(Hdpa)_2(dpq)]^{2+}$ displays a peak at m/z = 337.6, calc. 337.8. ^{1}H NMR (DMSO-d_6, 400 MHz): δ (multiplicity, integration, assignment, J/Hz, c.i.s.)/ppm. Group I, 9.129 (d, 2H, H_2, 7.5, −0.303), 9.123 (t, 2H, H_3, 4.4, 1.200), 9.559 (d, 2H, H_4, 7.7, 0.338), 9.374 (s, 2H, H_6, 0.240). Group II, 7.315 (d, 2H, H_3, 8.3, −0.422), 8.163 (t, 2H, H_4, 4.1, 0.527), 7.588 (t, 2H, H_5, 6.3, 0.741), 7.685 (d, 2H, H_6, 4.8, −0.528). Group III, 7.023 (d, 2H, H_3, 8.1, −0.714), 7.985 (t, 2H, H_4, 4.2, 0.349), 6.483 (t, 2H, H_5, 6.3, −0.364), 7.038 (d, 2H, H_6, 4.4, −1.175) and 10.611 (s, 2H, NH, 0.979).

Synthesis of [Ru(Hdpa)$_2$(mdpq)](ClO$_4$)$_2$ 4. This was prepared by refluxing *cis*-[Ru(Hdpa)$_2$(Cl$_2$)]Cl (0.15 g, 0.26 mmol) and mdpq (0.064 g, 0.26 mmol) using the procedure employed for **1**. Yield: 0.16 g (72%). Anal. Calc. for $RuC_{35}H_{28}N_8Cl_2O_8$: C, 47.31; H, 3.18; N, 15.76. Found: C, 47.10; H, 3.08; N, 15.25%. λ_{max}/nm (ε/M^{-1} cm^{-1}) (5% CH_3OH–5 mM Tris-HCl–50 mM NaCl buffer (0.5 : 9.5, v/v) buffer at pH 7.1): 525 (sh), 463 (5895), 435 (sh) (6094), 371 (7889), 282 (52 982), 260 (61 621). ESI-MS: $[Ru(Hdpa)_2(mdpq)]^{2+}$ displays a peak at m/z = 344.6, calc. 344.8. ^{1}H NMR (DMSO-d_6, 400 MHz): δ (multiplicity, integration, assignment, J/Hz, c.i.s.)/ppm. Group I, 9.123 (d, 2H, H_2, 8.0, −0.343), 9.119 (t, 2H, H_3, 4.5, 1.257), 9.536 (d, 2H, H_4, 6.3, 0.325), 9.507 (d, 2H, $H_{4'}$, 6.1, 0.296), 9.274 (s, 1H, H_6, 0.238), 2.941 (s, 3H, CH_3, 0.143). Group II, 7.300 (d, 2H, H_3, 8.2, −0.437), 8.137

(t, 2H, H_4, 5.4, 0.501), 7.581 (t, 2H, H_5, 6.4, 0.734), 7.693 (d, 2H, H_6, 4.9, −0.520). Group III, 7.000 (d, 2H, H_3, 8.2, −0.737), 7.985 (t, 2H, H_4, 5.5, 0.349), 6.481 (t, 2H, H_5, 6.3, −0.366), 7.022 (d, 2H, H_6, 4.6, −1.191) and 10.574 (s, 2H, NH, 0.942).

Synthesis of [Ru(Hdpa)$_2$(dppz)](ClO$_4$)$_2$ 5. This was prepared by refluxing *cis*-[Ru(Hdpa)$_2$(Cl$_2$)]Cl (0.2 g, 0.35 mmol) and dppz (0.099 g, 0.35 mmol) using the procedure employed for **1**. Yield: 0.25 g (80%). Anal. Calc. for $RuC_{38}H_{28}N_8Cl_2O_8$: C, 49.36; H, 3.05; N, 15.15. Found: C, 49.15; H, 3.03; N, 15.05%. λ_{max}/nm (ε/M^{-1} cm^{-1}) (5% CH_3OH–5 mM Tris-HCl–50 mM NaCl buffer (0.5 : 9.5, v/v) buffer at pH 7.1): 479 (4279), 437 (sh) (4623), 373 (13 814), 360 (14 081), 279 (56 256). ESI-MS: [Ru(Hdpa)$_2$(dppz)]$^{2+}$ displays a peak at m/z = 362.6, calc. 362.9. ^{1}H NMR (DMSO-d_6, 400 MHz): δ (multiplicity, integration, assignment, J/Hz, c.i.s.)/ppm. Group I, 9.081 (d, 2H, H_2, 8.0, −0.376), 8.641 (t, 2H, H_3, 4.5, 0.736), 9.643 (d, 2H, H_4, 5.3, 0.461), 8.226 (d, 2H, H_7, 5.8, −0.103), 8.143 (t, 2H, H_8, 6.3, 0.113). Group II, 7.326 (d, 2H, H_3, 8.2, −0.411), 7.987 (t, 2H, H_4, 4.4, 0.351), 7.043 (t, 2H, H_5, 6.4, 0.196), 7.678 (d, 2H, H_6, 4.5, −0.535). Group III, 7.074 (d, 2H, H_3, 8.2, −0.663), 7.613 (t, 2H, H_4, 4.5, −0.023), 6.513 (t, 2H, H_5, 6.5, −0.334), 7.109 (d, 2H, H_6, 4.8, −1.104) and 10.686 (s, 2H, NH, 1.054). ESI-MS: [Ru(Hdpa)$_2$(dppz)]$^{2+}$ displays a peak at m/z = 362.6, calc. 362.9.

X-Ray crystallography

A crystal of **1** of suitable size was selected from the mother-liquor and immersed in paraffin oil, then mounted on the tip of a glass fiber and cemented using epoxy resin. Intensity data for crystal was collected using Mo-Kα (λ = 0.71073 Å) radiation on a Bruker SMART APEX diffractometer equipped with CCD area detector at 100 K. The data integration and reduction was processed with SAINT[24] software. An empirical absorption correction was applied to the collected reflections with SADABS.[25] The structure was solved by direct methods using SHELXTL[26] and was refined on F^2 by the full-matrix least-squares technique using the SHELXL-97[27] program package. All non-hydrogen atoms were refined anisotropically till convergence is reached. Hydrogen atoms attached to the ligand moieties are stereochemically fixed. The crystallographic data and details of data collection for **1** is given in Table 1. Graphical representations of the structure were made with POV-Ray v3.6.[28]

DNA binding experiments

Concentrated stock solutions of metal complexes were prepared by dissolving them in 5% CH_3OH–5 mM Tris-HCl–50 mM NaCl buffer (0.5 : 9.5, v/v) buffer at pH 7.1 of metal complexes and diluting suitably with corresponding buffer to required concentrations for all the experiments. For absorption and emission spectral experiments the DNA solutions were pretreated with the solutions of metal complexes to ensure no change in concentration of the metal complexes. The absorption spectra were recorded on a Varian Cary 300 Bio UV-Vis spectrophotometer using cuvettes of 1 cm path length.

Absorption spectral titration experiments were performed by maintaining a constant concentration of the complex and varying the nucleic acid concentration. This was achieved by dissolving an appropriate amount of the metal complex and DNA stock solutions while maintaining the total volume constant (1 mL). This results in a series of solutions with varying concentrations of DNA but with a constant concentration of the complex. The absorbance (A) was recorded after successive additions of CT DNA.

Table 1 Crystal data and structure refinement details for **1**

Empirical formula	$RuC_{32}H_{25}N_8Cl_2O_8$
M_r	821.57
Crystal system	Orthorhombic
Space group	*Pbca*
a/Å	18.642(10)
b/Å	15.952(9)
c/Å	22.343(12)
V/Å^3	6644(6)
Z	8
D_c/g cm^{-3}	1.643
μ/cm^{-1}	6.98
λ(Mo-Kα)/Å	0.71073
T/K	293(2)
F(000)	3320
Reflection collected	24624
Independent reflections	4333
R_{int}	0.2366
Goodness-of-fit on F^2	1.057
R^a ($I \geq 2\sigma(I)$)	0.0936
wR^b ($I \geq 2\sigma(I)$)	0.2158

$^a R = \sum\|F_o\| - |F_c\|/\sum|F_o|$. $^b R = (\sum[w(|F_o| - |F_c|)^2/\sum[w(|F_o|)^2]\}^{1/2}$.

For viscosity measurements a Schott Gerate AVS 310 automated viscometer was thermostated at 25 ± 1 °C in a constant temperature bath. DNA concentration was kept constant (200 μM in NP) and the concentration of metal complexes varied ($1/R$ = [Ru]/[DNA] = 0.0–0.50). The flow times were noted from the digital timer attached with the viscometer. Data are presented as η/η_0 *vs.* $1/R$, where η is the viscosity of DNA in the presence of the ruthenium(II) complex and η_0 is the relative viscosity of DNA alone. Relative viscosity values were calculated from the observed flow time of DNA solution (t) corrected for the flow time of buffer alone (t_0), using the expression $\eta_0 = (t - t_0)/t_0$.

Circular dichroic spectra of DNA were obtained by using JASCO J-716 spectropolarimeter equipped with a Peltier temperature control device. All experiments were done using a quartz cell of 1 cm path length for DNA or 0.2 cm path length for oligonucleotides. Each CD spectrum was collected after averaging over at least four accumulations using a scan speed of 100 nm min^{-1} and a 1 s response time. Machine plus cuvette baselines were subtracted and the resultant spectrum zeroed 50 nm outside the absorption bands. Emission intensity measurements were carried out using Jasco F 6500 spectrofluorimeter. The tris buffer was used as a blank to make preliminary adjustments. The excitation wavelength was fixed and the emission range was adjusted before measurements. DNA was pretreated with ethidium bromide in the ratio [NP/EthBr] = 10 for 30 min at 27 °C. The metal complexes ($1/R$ = [metal]/[DNA] = 10) were then added to this mixture and their effect on the emission intensity was measured. Cyclic voltammetry (CV) and differential pulse voltammetry (DPV) were performed in a single compartment cell with a three-electrode configuration on a EG & G PAR 273 potentiostat-galvanostat equipped with an PIV computer. The working electrode was a glassy carbon disk (0.384 cm^2) and the reference electrode a

saturated calomel electrode. A platinum plate was used as the counter electrode. The supporting electrolyte was 50 mM NaCl–5 mM Tris-HCl buffer at pH 7.1. Solutions were deoxygenated by purging with nitrogen gas for 15 min prior to measurements; during measurements a stream of N_2 gas was passed over the solution. All the experiments were carried out at 25.0 ± 0.2 °C maintained by a Haake D8-G circulating bath. The redox potential $E_{1/2}$ was calculated from the anodic (E_{pa}) and cathodic (E_{pc}) peak potentials of CV traces as $(E_{pa} + E_{pc})/2$ and also from the peak potential (E_{pa}) of DPV response as $E_p + \Delta E/2$ (ΔE is the pulse height).

The interaction of complexes with supercoiled pBR322 DNA was monitored using agarose gel electrophoresis. In reactions using supercoiled pBR322 plasmid DNA (Form I, 40 μM) in 5% CH_3OH–5 mM Tris-HCl–50 mM NaCl buffer (0.5 : 9.5, v/v) at pH 7.1 was treated with metal complexes in the same buffer. For photocleavage studies, the reactions were carried out under illuminated conditions at 365 nm (12 W) monochromatic light source. In each experiment supercoiled pBR322 DNA (Form I, 40 μM) was treated with metal complexes (60 μM) and irradiated at 365 nm monochromatic wavelength for 5 min. The samples were then incubated for 1 h in the dark for 37 °C and analysed for the photocleaved products using gel electrophoresis as discussed below. A loading buffer containing 25% bromophenol blue, 0.25% xylene cyanol and 30% glycerol (3 μl) was added and electrophoresis performed at 60 V for 5 h in Tris–acetate–EDTA (TAE) buffer (40 mM Tris-base, 20 mM acetic acid, 1 mM EDTA) using 1% agarose gel containing 1.0 μg mL^{-1} ethidium bromide.[29] The gels were viewed in a Gel doc system and photographed using a CCD camera (Alpha Innotech Corporation).

Cell viability assay

MTT assay was carried out as described previously.[30] The complexes **1–5**, in the concentration 0.05–100 μM, dissolved in DMSO (Sigma-Aldrich, St. Louis, MO, USA), were added to the wells 24 h after seeding of 5×10^3 cells per well in 200 μL of fresh culture medium. DMSO was used as the vehicle control. After 24 and 48 h, 20 μL of MTT solution [5 mg/mL in phosphate-buffered saline (PBS)] was added to each well and the plates were wrapped with aluminum foil and incubated for 4 h at 37 °C. The purple formazan product was dissolved by addition of 100 μL of 100% DMSO to each well. The absorbance was monitored at 570 nm (measurement) and 630 nm (reference) using a 96 well plate reader (Bio-Rad, Hercules, CA, USA). The stock solutions of the metal complexes were prepared in DMSO and in all the experiments the percentage of DMSO was maintained in the range of 0.1–1%. DMSO by itself was found to be non-toxic to the cells till 1% concentration. Data were collected for four replicates each and used to calculate the mean. The percentage inhibition was calculated, from this data, using the formula:

$$= \frac{\text{Mean OD of untreated cells (control)} \quad \text{Mean OD of treated cells}}{\text{Mean OD of untreated cells (control)}} \times 100$$

The IC_{50} values were calculated using Table Curve 2D version 5.01.

Hoechst 33258 staining

Cell pathology was detected by staining the nuclear chromatin of trypsinized cells (4.0×10^4 ml^{-1}) with 1 μl of Hoechst 33258 (1 mg ml^{-1}, aqueous) for 10 min at 37 °C. Protocol: Staining of suspension cells with Hoechst 33258 to detect apoptosis.[31] A drop of cell suspension was placed on a glass slide and a cover-slip was laid over to reduce light diffraction. At random 300 cells were observed in a fluorescent microscope (Carl Zeiss, Jena, Germany) fitted with a 377–355 nm filter, and observed at ×400 magnification and the percentage of cells reflecting pathological changes were calculated. Data were collected for four replicates and used to calculate the mean and the standard deviation.

Results and discussion

Synthesis and characterisation of Ru(II) complexes

The mixed ligand complexes $[Ru(Hdpa)_2(diimine)](ClO_4)_2$ **1–5**, where Hdpa is 2,2′-dipyridylamine and diimine is 1,10-phenanthroline (phen) (**1**), 5,6-dimethyl-1,10-phenanthroline (5,6-dmp) (**2**), dipyrido[3,2-*d*:2′,3′-*f*]quinoxaline (dpq) (**3**), 5-methyldipyrido[3,2-*d*:2′,3′-*f*]quinoxaline (mdpq) (**4**) and dipyrido[3,2-*a*:2′,3′-*c*]phenazine (dppz) (**5**) have been isolated by reacting the complex $[Ru(Hdpa)_2Cl_2]Cl$ with the corresponding diimine ligands. The CHN analyses of the complexes were consistent with the formula $[Ru(Hdpa)_2(diimine)](ClO_4)_2$. The complexes are soluble in both polar and non-polar solvents. The perchlorate salts of **3–5** are highly soluble in water but those of **1** and **2** are soluble in 5% CH_3OH–5 mM Tris-HCl–50 mM NaCl buffer (0.5 : 9.5, v/v) at pH 7.1. So solutions of the all complexes were prepared in 5% CH_3OH–5 mM Tris-HCl–50 mM NaCl buffer at pH 7.1 for DNA binding and other studies.

Description of the structure of $[Ru(Hdpa)_2(phen)](ClO_4)_2$ (1). The ball-and-stick representation of the structure of the cation $[Ru(Hdpa)_2(phen)]^{2+}$ of complex **1** is illustrated in Fig. 1 with atom numbering scheme. The crystallographic data are given in

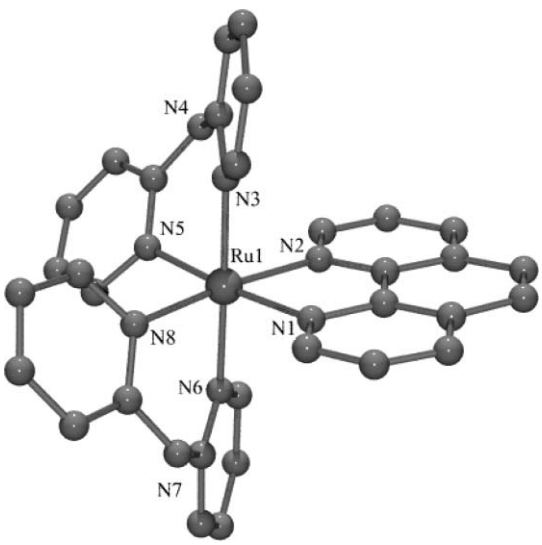

Fig. 1 Ball-and-stick representation of the crystal structure of $[Ru(Hdpa)_2(phen)]^{2+}$ cation **1**; atoms as spheres of arbitrary diameter. Hydrogen atoms are omitted for clarity.

Table 2 Selected interatomic distances (Å) and angles (°) for **1**

Ru(1)–N(1)	2.086(10)	Ru(1)–N(4)	2.051(11)
Ru(1)–N(2)	2.084(9)	Ru(1)–N(5)	2.072(11)
Ru(1)–N(3)	2.073(11)	Ru(1)–N(6)	2.071(11)
N(1)–Ru(1)–N(2)	79.7(4)	N(2)–Ru(1)–N(8)	173.0(5)
N(1)–Ru(1)–N(3)	88.5(4)	N(3)–Ru(1)–N(5)	88.5(5)
N(1)–Ru(1)–N(5)	175.0(4)	N(3)–Ru(1)–N(6)	177.9(5)
N(1)–Ru(1)–N(6)	93.6(4)	N(3)–Ru(1)–N(8)	93.3(5)
N(1)–Ru(1)–N(8)	74.1(4)	N(5)–Ru(1)–N(6)	89.4(4)
N(2)–Ru(1)–N(3)	89.7(4)	N(5)–Ru(1)–N8	89.9(4)
N(2)–Ru(1)–N(5)	96.4(4)	N(6)–Ru(1)–N8	86.9(5)
N(2)–Ru(1)–N(6)	90.3(4)		

Table 1 while the selected bond lengths and bond angles are given in Table 2. The complex cation possesses a distorted octahedral coordination geometry constituted by two dipyridylamine (Hdpa) and 1,10-phenanthroline ligands chelated to Ru(II). The presence of distorted coordination geometry around Ru(II) is evident from the values of the bond angles N1–Ru1–N2 [79.6(4)], N1–Ru1–N3 [88.5(4)], N6–Ru1–N8 [87.0(5)], N3–Ru–N6 [177.9(5)], N2–Ru1–N8 [173.0(6)] and N1–Ru1–N5 [175.0(4)°], which deviate from the ideal bond angles of 90° and 180°. The pyridyl rings of the coordinated Hdpa ligands are non-planar to each other. The least squares planes of the pyridyl rings of the first Hdpa ligand coordinated to the metal center shows an interplanar angle (N3–C13 to C17 and N5–C19 to C22) of 35.19°, which is higher than that (39.66°) between the pyridyl rings of the second Hdpa ligand (N6–C23 to C27 and N8–C28 to C32) suggesting that the first Hdpa ligand makes a more effective coordination than the second one and that the steric crowding of ligands is significant. The flexible non-planar Hdpa ligands approach Ru(II) more closely and σ-coordinates to Ru(II) more strongly than the rigid 1,10-phenanthroline ligand. A similar observation has been made earlier.[32] The Ru–N_{Hdpa} and Ru–N_{phen} bond distances are very similar to those observed in other Hdpa and phen complexes.[33,34]

^{1}H NMR spectra

The ^{1}H NMR spectra[35,36] of **1–5** contain mainly eleven distinct resonances (six doublets and five triplets), which could be classified into three groups (group I, H_2–H_4, group II and III, H_3–H_6; Scheme 1 and Fig. S1, ESI†). The group I has three resonances which arise from coupling of H_2, H_3 and H_4 protons of phen ring with each other. Similarly, the groups II and III have each four resonances, which arise from coupling of H_3, H_4, H_5 and H_6 protons of Hdpa with each other. When coordinated to Ru(II) the planar phen, 5,6-dmp, dpq, mdpq and dppz rings are expected to form a five-membered chelate ring with an envelope conformation and the non-planar Hdpa ligands form six-membered chelate rings[32] with a boat conformation, as observed in the X-ray crystal structure of **1**. A combination of conformations of the two Hdpa ligands gives four cases as shown in Fig. 2. For cases 2 and 3, the chemical shifts should be different among the two halves of the phen ring and also among the four pyridine rings of Hdpa ligand because of absence of flapping of the pyridine rings of the ligand. On the other hand, for cases 1 and 4 three groups of magnetic environments – two equivalent halves of phen and four pyridine rings of Hdpa – would arise because of flapping of the py rings of Hdpa and hence the presence of a C_2 symmetry. The

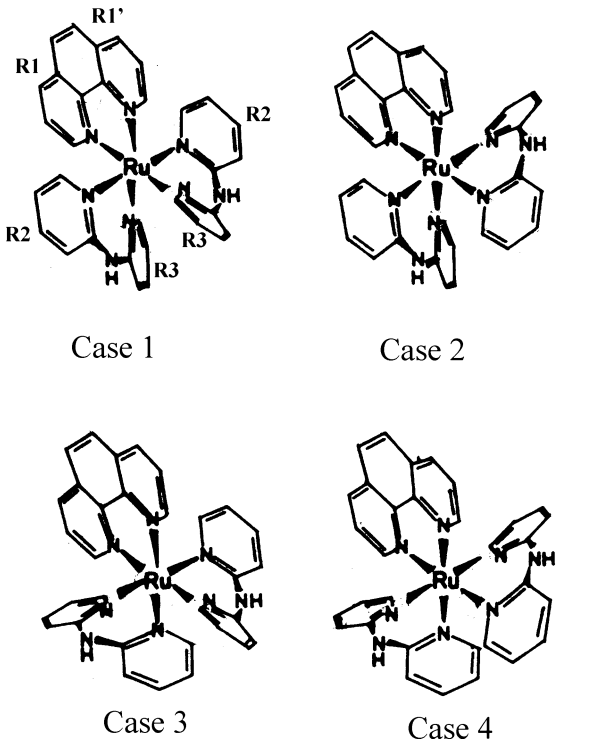

Fig. 2 The numbering of the phen and pyridine rings of Hdpa ligands and four cases due to the conformation of the Hdpa ligands in $[Ru(Hdpa)_2(phen)]^{2+}$ (**1**)

observed ^{1}H NMR spectral pattern is consistent with cases 1 and 4, suggesting the presence of C_2 symmetry and hence the rapid flapping of the py rings of Hdpa ligand. Also, the X-ray crystal structure of **1** reveals no steric interaction between H_6 and $H_{6'}$ protons of the Hdpa ligands occupying *cis* positions and supports the presence of rapid flapping of Hdpa ligands with no inhibition from ligand crowdedness. Thus, the two halves of phen/5,6-dmp/dpq/mdpq/dppz ring (R1 and R1′) in **1–5** with an apparent C_2 symmetry become equivalent and also the two pyridine rings of Hdpa1-R2 and Hdpa1-R3 become equivalent to Hdpa2-R2 and Hdpa2-R3, respectively. However, the current-loop model calculation[37] of aromatic ring-current shifts of $[Ru(Hdpa)_2(bpy)]^{2+}$ indicates that the flapping of Hdpa ligands makes each proton of the complex experience an averaged magnetic environment among cases 1–4.

The chemical shifts of each proton in 5,6-dmp (**2**) or dpq (**3**) or mdpq (**4**) or dppz (**5**) are related (Fig. S2B, ESI†) to that of phen (**1**) whereas the proton signals of Hdpa (**2–5**) are in good agreement (Fig. S2C and S2D, ESI†) with those of Hdpa in **1**. Judging by the similarity of the patterns with the homoleptic complexes[38] $[Ru(phen)_3]^{2+}$ and $[Ru(Hdpa)_3]^{2+}$ as well as **1** (Fig. S2A, ESI†), group I can be assigned to R1 of the phen or 5,6-dmp or dpq or mdpq or dppz ligand, while groups II and III are assigned to either R2 or R3 of Hdpa ligands. Apart from the three main resonances of group I, the complexes **1**, **2** and **3** show one individual resonance for the benzene ring (H_5) of phen, dimethyl substituted benzene ring (CH_3) of 5,6-dmp and quinoxaline ring (H_6) of dpq. Similarly, **4** and **5** exhibit two individual resonances for the methyl substituted quinoxaline ring (H_6 and CH_3) of mdpq and phenazine ring (H_7 and H_8) of dppz.

The complexes **1–5** exhibit negative c.i.s. values for H_2 (group I) and H_6 (group II and III) protons adjacent to the coordinated nitrogen atoms, which result from through space ring-current anisotropy effects upon coordination, with the protons lying directly over the shielding plane of another aromatic pyridine ring. Also, upon coordination to Ru(II), the signals of H_7 (**5**; group I), H_3 (**1–5**; group II and III), H_4 (**1**, **2**, **5**; group III) and H_5 (**1–5**; group III) protons are shifted upfield due to Ru(II)-to-ligand π-back donation. The positive c.i.s. values observed for H_3 and H_4 (**1–5**; group I), H_5 (**1**, **2**; group I), H_6 (**3**, **4**; group I), H_8 (**5**; group I), H_4 and H_5 (**1–5**; group II) and H_4 (**3**, **4**; group III) protons arise from a σ-effect based on electron donation to Ru(II) *via* the nitrogen lone pairs.

Interaction of Ru(II) complexes with DNA

Absorption spectral studies

In 5% CH_3OH–5 mM Tris-HCl–50 mM NaCl buffer at pH 7.1 the complexes **1–5** display a higher energy band in the range 230–380 nm, which arises from intra-ligand π–π* type transitions[39] involving ligand energy levels higher in energy than the ligand LUMO levels. The MLCT bands for **1–5** all appear in the region of the spectrum typical for Ru(II) complexes with coordinated polyimine ligands. The MLCT band energy decreases from phen complex **1** (451 nm) to dppz complex **5** (484 nm) with 33 nm red-shifted, as the diimine ligand is replaced by one with enhanced π-delocalization revealing stabilization of the π* (diimine-based LUMO).[40] The methyl substitution on phen co-ligand would be expected to build a negative charge on metal by σ-donating methyl groups to destabilize the π* (diimine-based LUMO), but it is not observed in the dmp complex **2**. However, methyl substitution on dpq co-ligand destabilizes the π* orbital (diimine-based LUMO) and decreases (3 nm) the metal $d\pi(Ru^{II}) \rightarrow \pi^*$ MLCT band energy relative to the analogous dpq complex **3**. Except **5**, the complexes **1–4** display a new lower energy band in the range 505–525 nm, which arises from inter-ligand n_{Hdpa}–$\pi^*_{diimine}$.[39] The complexes **1–5** exhibit no detectable luminescence in 5% CH_3OH–5 mM Tris-HCl–50 mM NaCl buffer at pH 7.1.

Upon the addition of calf thymus (CT) DNA to **1–5** (R = [NP]/[Ru complex] = 0–25) in 5% CH_3OH–5 mM Tris-HCl–50 mM NaCl buffer at pH 7.1 at 25 °C interesting changes in intensity of the intense intraligand (IL) absorption bands (264–387 nm) and metal-to-ligand ($\pi_M \rightarrow \pi_L^*$) charge transfer (MLCT) band of the complexes in the visible region (453–484 nm, Table 3) are observed. All the complexes exhibit uniform hypochromism at lower DNA concentrations but hyperchromism[41] at higher DNA concentrations revealing that the DNA binding modes of all the complexes are similar (Fig. 3). It appears that the complexes undergo distortion in the coordination sphere at higher DNA concentrations resulting in enhanced allowedness of the intraligand as well as MLCT bands. The mixed spectral behaviour reveals the presence of more than one DNA binding mode for the complexes. Also, while the well defined MLCT bands observed for **1–4** were used to monitor absorption titration of the complexes, the intraligand transition was used for **5**. So no attempt was made to quantitatively compare the DNA binding affinities of the complexes. The higher hypochromism exhibited by **5** is obviously due to involvement of the extended aromatic ring of dppz ligand in intercalative interaction with the DNA base pairs. Also, as expected, the methyl substituted 5,6-dmp and mdpq complexes **2** and **4** show lower hypochromism than their analogous phen (**1**) and dpq (**3**) complexes (*cf*. below).

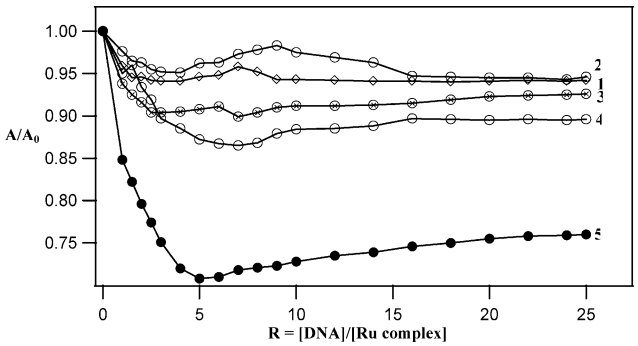

Fig. 3 Effect of addition of DNA on the absorption intensity of the complexes **1**, 453; **2**, 453; **3**, 446; **4**, 464; **5**, 484 nm in a 5% CH_3OH–5 mM Tris-HCl–50 mM NaCl buffer at pH 7.1 and 25 °C.

Ethidium displacement assay

All the present complexes fail to show steady-state emission in 5% CH_3OH–5 mM Tris-HCl–50 mM NaCl buffer at pH 7.1 at 25 °C and lack emission even in the presence of CT DNA (R = 25). So the extent of DNA binding of these complexes has been evaluated using competitive binding studies involving ethidium bromide (EthBr), which is known to emit strongly (λ_{ex}, 450; λ_{em}, 595 nm) due to its intercalative interaction with DNA. On adding the complexes **1–5** to DNA (R = 1) pretreated with EthBr ([DNA]/[EthBr]) = 1) the emission intensity decreases (Fig. 4). The observed fluorescence intensities of DNA-bound ethidium bromide were plotted against complex concentration and the

Table 3 Absorption spectral properties of Ru(II) complexes bound[a] to CT DNA

Complex	λ_{max}/nm	R	Change in absorbance	Δε (%)	Red shift/nm
$[Ru(Hdpa)_2(phen)]^{2+}$ **1**	453	25	Hypo- and hyperchromism	6	5
$[Ru(Hdpa)_2(5,6\text{-}dmp)]^{2+}$ **2**	453	25	Hypo- and hyperchromism	5	2
$[Ru(Hdpa)_2(dpq)]^{2+}$ **3**	446	25	Hypo- and hyperchromism	18	1
$[Ru(Hdpa)_2(mdpq)]^{2+}$ **4**	464	25	Hypo- and hyperchromism	11	9
$[Ru(Hdpa)_2(dppz)]^{2+}$ **5**	484	25	Hypo- and hyperchromism	14	2

[a] Measurement were made at R = 25, where R = [DNA]/[Ru complex], concentration of Ru(II) complex solutions = 1×10^{-4} M (**1**, **2** and **4**) and 5×10^{-5} M (**3** and **5**).

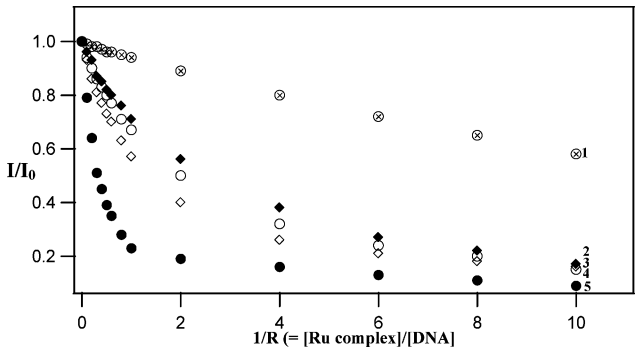

Fig. 4 Effect of addition of **1–5** on the emission intensity of the CT DNA-bound ethidium bromide (125 μM) at different complex concentrations in a 5% CH_3OH–5 mM Tris-HCl–50 mM NaCl buffer at pH 7.1 and 25 °C.

values of apparent DNA binding constant (K_{app}) were calculated[42] using the relation

$$K_{EthBr}[EthBr] = K_{app}[Complex]$$

where,[42] K_{EthBr} is 1.0×10^7 M^{-1}, the concentration of EthBr is 12.5 μM and the concentration of the complex is that used to obtain a 50% reduction of fluorescence intensity of EthBr. The DNA binding abilities of the complexes follow the order, **5** dppz (K_{app}, 9.78×10^7 M^{-1}) > **3** dpq (5.84×10^7 M^{-1}) > **4** mdpq (5.00×10^7 M^{-1}) > **2** dmp (4.77×10^7 M^{-1}) > **1** phen (0.97×10^7 M^{-1})). Both the electron transfer from excited EthBr to ruthenium(II) and the EthBr displacement mechanisms would account for the highest K_{app} value of the dppz complex (*cf.* below) and hence its DNA binding affinity as well (*cf*. above). The dppz complex **5**, which is involved in a strong DNA intercalation, would compete with the intercalatively bound EthBr for DNA binding and quench the EthBr emission to a greater extent (100%) than other complexes. It appears that the DNA helix simultaneously accommodates both the complex and EthBr in the grooves and the enhanced hydrophobicity of the fused benzene ring in DNA-bound dppz complex perturbs the DNA helix more than the other complexes, to displace the bound EthBr more efficiently. This is attributed to the intramolecular photoinduced electron transfer exhibited by the flanking phenazine moiety in DNA-bound or free dppz complex quenches the emission of the DNA-bound EthBr.[43] The phen complex **1**, which is involved in partial DNA intercalation, would be expected to show a K_{app} value higher than **2**. However, **2** shows a K_{app} value higher than **1** indicating that the hydrophobic interaction[34] of **2** with DNA involving 5,6 methyl groups rather than the partial intercalation of phen ring is more important in determining the EthBr quenching. The complex **4** displays a K_{app} value lower than **3** even though it possesses one methyl group on the quinoxaline moiety. So two adjacent methyl groups are needed to place them effectively in the grooves and displace the DNA-bound EthBr.[44] The dicationic complex **5** is expected to be involved in strong partial intercalation with DNA and compete with the intercalatively bound monopositive ethidium cation more strongly than other complexes. We propose that hydrogen bonding interactions, which would occur between the–NH- of Hdpa in **5** and functional groups present on the edge of the DNA,[1c] would also contribute significantly to the higher DNA binding affinity of **5**.

Circular dichroic spectral studies

Circular dichroic spectra provide information about the chirality of spectroscopically active species in solution and this is a useful technique in diagnosing changes in DNA morphology during drug–DNA interactions, as the band due to base stacking (275 nm) and that due to right-handed helicity (248 nm) are quite sensitive to the mode of DNA interactions with small molecules.[45] The changes in CD signals of DNA observed on interaction with drugs may often be assigned to the corresponding changes in DNA structure.[46] Thus simple groove binding and electrostatic interaction of small molecules show less or no perturbation on the base-stacking and helicity bands, while intercalation enhances the intensities of both the bands stabilizing the right-handed B conformation of CT DNA as observed for the classical intercalator methylene blue.[47] Thus *rac*-metal complexes give a zero CD but show induced circular dichroic (ICD) signals on enantiopreferential binding to DNA providing further and definitive confirmation for their DNA binding.[48,49] Thus, the CD spectral technique has been used to study the enantiopreferential DNA binding of the present *rac*-metal complexes. Also, the technique is useful in diagnosing changes in DNA morphology during drug-DNA interaction as CD signals are quite sensitive to the mode of DNA interactions of small molecules.[43,50]

When the present *rac*-complexes are incubated with CT DNA at $1/R$ (= [Ru complex]/[DNA]) value of 1, the CD spectrum of DNA undergoes changes in both the positive and negative bands (Table 4). Upon adding complex **1** slight changes in intensities of the negative and positive bands, and shifts in band positions are observed. This reveals that **1** merely binds with DNA electrostatically. Interestingly, **2** shows a sharp B to Ψ conformational change (Fig. 5), which is similar to that observed for $[Co(NH_3)_6]^{3+}$ bound to DNA of short lengths with 160 base pairs.[51] On the other hand, upon addition of *rac* complexes **3** (Fig. 6), **4** (Fig. 7) and **5** (Fig. 8) to DNA both these bands disappear and an inverted CD signal is observed with intensity much higher than free DNA. The latter consists of a positive (262 nm) and a negative band (282 nm) with a zero cross-over at 272 nm. This is typical of exciton coupled ICD arising due to enantiopreferential binding of the Δ-enantiomer of the *rac*-complex and/or ligand–ligand interactions among DNA bound/unbound complexes. The complexes **3–5** which exhibits ICD interact with different polynucleotides and the binding efficiency varies as CT DNA > $poly(AT)_{12}$ ≅ $d(CGCGATCGCG)_2$ > $poly(GC)_{12}$ (Fig. 6, 7 and

Table 4 CD parameters for the interaction of calf thymus DNA with complexes **1–5**

Sample	CD spectral band,[a] λ/nm	
50 μM CT DNA	245	276
DNA + 5 μM $[Ru(Hdpa)_2(phen)]^{2+}$ **1**	245	269
DNA + 5 μM $[Ru(Hdpa)_2(5,6\text{-dmp})]^{2+}$ **2**	245	267, 298
DNA + 5 μM $[Ru(Hdpa)_2(dpq)]^{2+}$ **3**	241, 286	262
DNA + 5 μM $[Ru(Hdpa)_2(mdpq)]^{2+}$ **4**	239, 286	263
DNA + 5 μM $[Ru(Hdpa)_2(dppz)]^{2+}$ **5**	243,289	264

[a] Measurement made at $1/R$ value of 1 for complexes **1–5** where $1/R$ = [Ru]/[NP]; concentration of DNA solutions = 5×10^{-5} M. Cell path length = 1 cm.

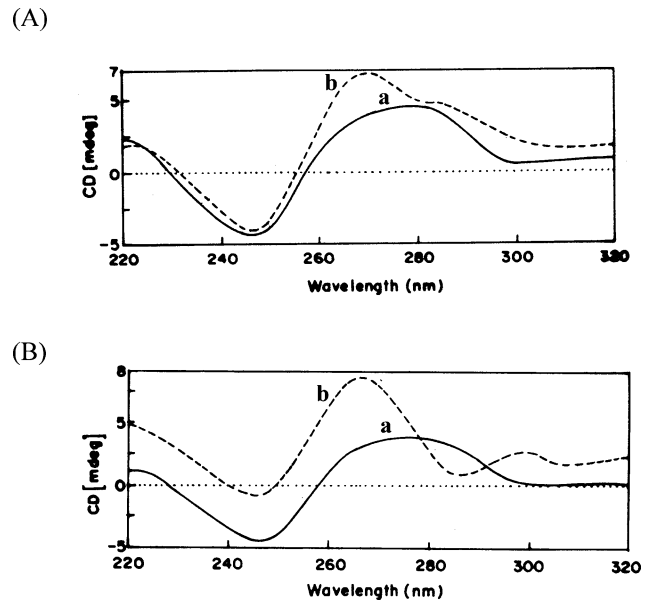

Fig. 5 (A) Circular dichroism spectra of CT DNA in the absence (a) and presence of $[Ru(Hdpa)_2(phen)]^{2+}$ (b) at $1/R = 1$. (B) Circular dichroism spectra of CT DNA in the absence (a) and presence of $[Ru(Hdpa)_2(5,6\text{-dmp})]^{2+}$ (b) at $1/R = 1$. [DNA] $= 2 \times 10^{-5}$ M.

8). These observations reveal the preferential binding of **3–5** to AT and mixed rather than GC sequences.

Viscometry studies

The hydrodynamic changes of DNA biopolymer are the consequence of lengthening of the molecule, the diminished bending between layers, and the diminished length-specific mass.[52] The DNA viscosity is enhanced significantly due to complete or partial intercalation of drugs into the DNA base stacking but it is slightly disturbed by electrostatic or covalent binding of molecules. When **1–5** are treated with CT DNA (200 μM) and their concentration is increased from $1/R = 0$–0.5 ($1/R$ = [Ru]/[DNA]), the relative viscosity of CT DNA increases (Fig. 9), which follows the order **5** > **3** > **4** > **2** > **1**. These results parallel the K_{app} values observed for the complexes and illustrate the lengthening of DNA duplex upon intercalation of the extended planar aromatic ligands of the complexes on DNA binding. The highest increase in DNA viscosity effected by **5** is similar to those observed for proven intercalators, and can be explained by a model used for the DNA binding of acridine orange and proflavine.[53] Also, incorporation of a methyl group on dpq in **3** decreases the partial intercalation of dpq leading to a lower increase in viscosity of DNA upon binding to **4**. On the other hand, the incorporation of two methyl group on phen ring as in 5,6-dmp leads to a higher increase in viscosity revealing the importance of hydrophobic interaction of **2** in DNA grooves in enhancing the length of DNA.

Electrochemical behaviour of complexes in the absence and presence of DNA

In 5% CH_3OH–5 mM Tris-HCl–50 mM NaCl buffer solution at pH 7.1 the complexes **1** and **2** exhibit a quasi-reversible Ru(II)/Ru(III) redox wave (ΔE_p, 98 mV) while **3–5** exhibit irreversible (ΔE_p, 172–232 mV) response (Table 5) with the $E_{1/2}$ values

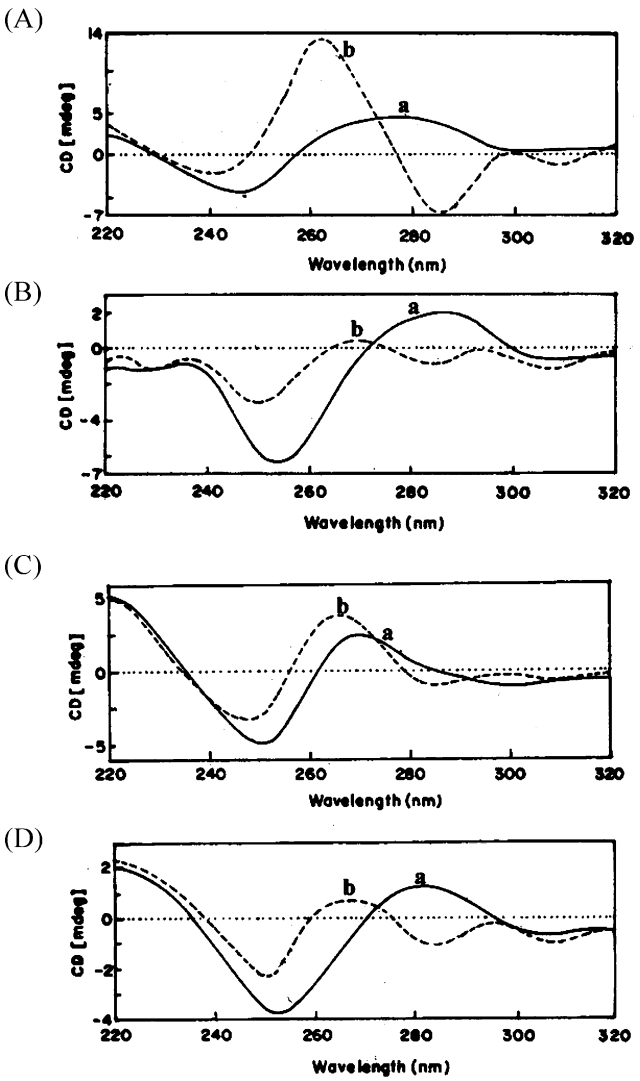

Fig. 6 (A) Circular dichroism spectra of CT DNA in the absence (a) and presence of $[Ru(Hdpa)_2(dpq)]^{2+}$ at $1/R = 1$; [DNA] $= 2 \times 10^{-5}$ M. (B) $poly(GC)_{12}$, (C) $poly(AT)_{12}$ and (D) $d(CGCGATCGCG)_2$ in the absence (a) and presence of $[Ru(Hdpa)_2(dpq)]^{2+}$ (b) at $1/R = 4$; $poly(GC)_{12}$, $poly(AT)_{12}$ and $d(CGCGATCGCG)_2 = 1 \times 10^{-5}$ M.

falling in the range of 0.555–0.630 V. In addition, all the complexes exhibit one more metal-based oxidative response in DPV with $E_{1/2}$ values falling in the range of 0.789–1.040 V. This is attributed to the Ru(II)/Ru(III) couple of deprotonated mixed-ligand complexes[54] $[Ru(dpa)_2(diimine)]$ as illustrated in Fig. 14 and Table 5. The low Ru(II)/Ru(III) redox potentials of the present chelates may be attributed to the strong σ-donating and less π-accepting ability of Hdpa ligand to stabilize the higher Ru(III) oxidation state. The formal potentials of the Ru(II)/Ru(III) couple $E^{\circ\prime}$ (or voltammetric $E_{1/2}$) follows the order **5** > **3** > **4** > **1** > **2**, which is in agreement with the MLCT band energies of the complexes (*cf.* above). The number of methyl groups and extended aromatic rings in the diimine ligands dictate the $E_{1/2}$ value and thus, incorporation of electron-repelling methyl groups on phen ring as in the 5,6-dmp complex **2** renders the oxidation of Ru(II) to Ru(III) facile leading to a $E_{1/2}$ values lower than the phen complex **1**. Similarly, the mdpq complex **4** exhibits the Ru(II)/Ru(III) redox couple at a potential lower than

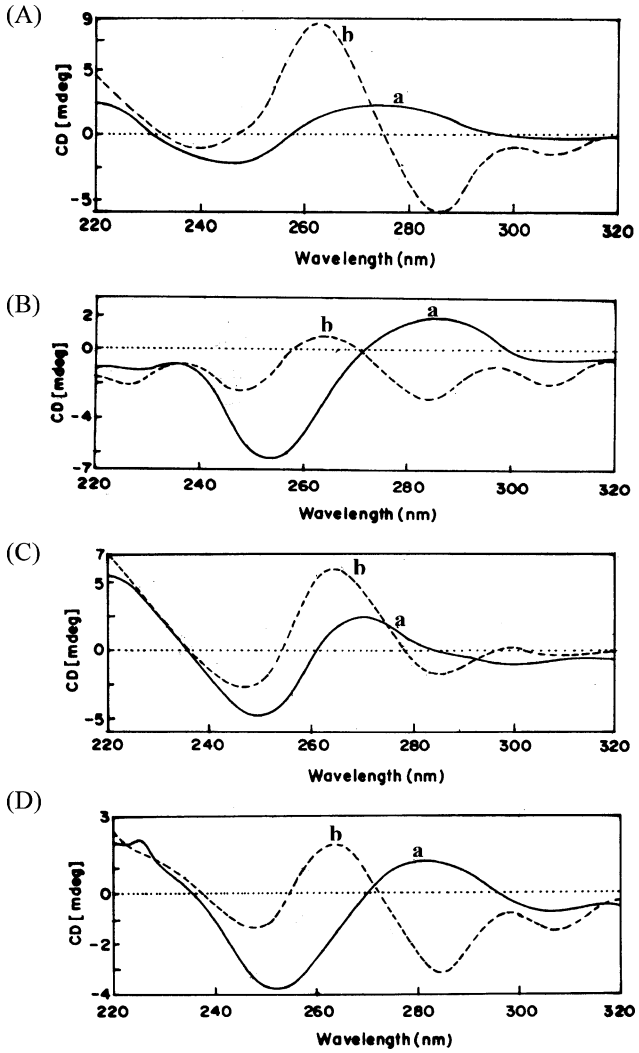

Fig. 7 (A) Circular dichroism spectra of CT DNA in the absence (a) and presence of $[Ru(Hdpa)_2(mdpq)]^{2+}$ at $1/R = 1$; [DNA] $= 2 \times 10^{-5}$ M. (B) poly(GC)$_{12}$, (C) poly(AT)$_{12}$ and (D) d(CGCGATCGCG)$_2$ in the absence (a) and presence of $[Ru(Hdpa)_2(mdpq)]^{2+}$ (b) at $1/R = 4$; poly(GC)$_{12}$, poly(AT)$_{12}$ and d(CGCGATCGCG)$_2$ $= 1 \times 10^{-5}$ M.

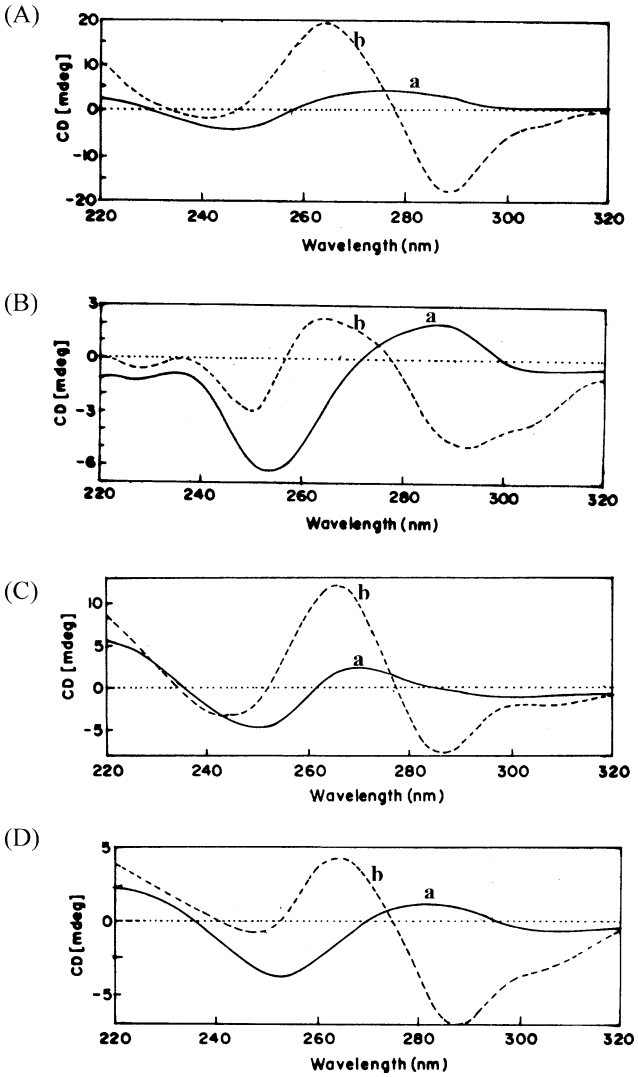

Fig. 8 (A) Circular dichroism spectra of CT DNA in the absence (a) and presence of $[Ru(Hdpa)_2(dppz)]^{2+}$ at $1/R = 1$; [DNA] $= 2 \times 10^{-5}$ M. (B) poly(GC)$_{12}$, (C) poly(AT)$_{12}$ and (D) d(CGCGATCGCG)$_2$ in the absence (a) and presence of $[Ru(Hdpa)_2(dppz)]^{2+}$ (b) at $1/R = 4$; poly(GC)$_{12}$, poly(AT)$_{12}$ and d(CGCGATCGCG)$_2$ $= 1 \times 10^{-5}$ M.

the dpq complex **3**. The Ru(II)/Ru(III) potentials become more positive as the diimine ligand is replaced by one with enhanced π-delocalization revealing the higher stabilization of the lower Ru(II) oxidation state, which is consistent with the decrease in MLCT band energy. All the complexes display one or two irreversible reduction waves in the potential range −0.349 to −1.559 V, which arise from addition of electrons in the electrochemically accessible LUMO[55] of the coordinated co-ligands rather than that of the Hdpa ligand.

The application of electrochemical methods to monitor the binding of metal complexes to DNA provides useful complements to the above methods of investigations such as UV-Vis and CD spectroscopy.[56] The cyclic (CV) and differential pulse voltammetric (DPV) responses have been obtained for **1–5** in 5% CH_3OH–5 mM Tris-HCl–50 mM NaCl buffer at pH 7.1 in the presence of DNA also and the well-behaved DPV responses are used to monitor the interaction of complexes with DNA (Table 5). On the incremental addition of CT DNA to the metal complexes ($R = 0.25$–3), an increase in peak currents of the anodic waves in the CV and DPV responses for **1–5** (Fig. 10) is observed at lower DNA concentrations. In contrast, at higher DNA concentrations the value of i_{pa} decreases. This indicates that multiple turnovers of oxidation of DNA by the oxidized Ru(III) form of the metal complexes occur during a single voltammetric sweep at lower DNA concentrations. The drop in peak currents at higher concentrations of DNA reveal the slower mass transfer of the complexes bound to DNA fragments, which leads to a decrease in concentration of the unbound redox-active species in solution. Similar catalytic enhancement of the anodic current has been observed on ITO electrode when complexes such as $[Ru(diimine)_3]^{2+}$, where diimine = bpy, phen and 5,6-dmp,[33,57] are interacted with CT DNA. A summary of the voltammetric results is given in Table 5 and the typical CV responses of the dpq complex in 5% CH_3OH–5 mM Tris-HCl–50 mM NaCl buffer in the presence and absence of CT DNA are shown in Fig. 10. It is

Table 5 Cyclic voltammetric behaviour[a] of Ru(II) complexes in the absence and presence of DNA at 25.0 ± 0.2 °C

Complex	R	E_{pa}/V	E_{pc}/V	$E_{1/2}$/V CV	$E_{1/2}$/V DPV (I)	$E_{1/2}$/V DPV (II)	ΔE_p/mV	$10^6 D$/cm^2 s^{-1}
$[Ru(Hdpa)_2(phen)]^{2+}$ **1**	0.00	0.631	0.533	0.582	0.580	1.040	98	7.0
	3.00	0.647	0.547	0.597	0.594	1.053	100	
					−0.349[b]	—		
$[Ru(Hdpa)_2(5,6\text{-dmp})]^{2+}$ **2**	0.00	0.620	0.522	0.571	0.577	0.798	98	0.14
	3.00	0.620	0.528	0.574	0.575	0.799	92	
					−1.311[b]	−1.559[b]		
$[Ru(Hdpa)_2(dpq)]^{2+}$ **3**	0.00	0.696	0.556	0.626	0.637	0.813	232	5.7
	3.00	0.710	0.522	0.616	0.667	0.839	188	
					−0.429[b]	−0.987[b]		
$[Ru(Hdpa)_2(mdpq)]^{2+}$ **4**	0.00	0.672	0.550	0.611	0.613	0.811	122	7.3
	3.00	0.704	0.500	0.602	0.681	0.816	204	
					−0.419[b]	−1.021[b]		
$[Ru(Hdpa)_2(dppz)]^{2+}$ **5**	0.00	0.730	0.558	0.644	0.655	0.829	172	0.12
	0.25	0.696	0.600	0.648	0.637	0.823	96	
					−0.557[b]	−0.757[b]		

[a] Measured *vs.* saturated calomel electrode; add 0.244 to convert to normal hydrogen electrode (NHE); scan rate 50 mV s^{-1}; supporting electrolyte 50 mM NaCl; complex concentration 0.25 × 10^{-3}; differential pulse voltammetry (DPV), scan rate 2 mV s^{-1}; pulse height 50 mV; R = [DNA]/[Ru(II) complex]. [b] Ligand reduction potential.

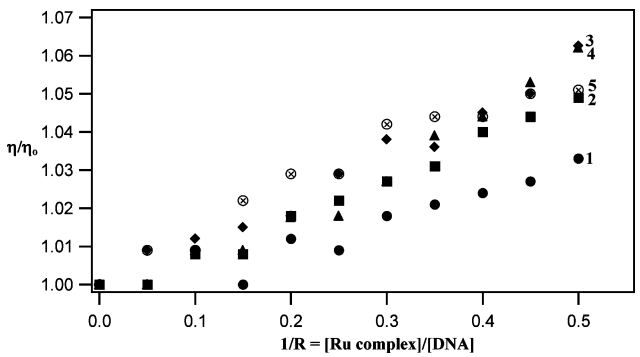

Fig. 9 The effect of addition of **1–5** on the viscosity of CT DNA in 5% CH_3OH–5 mM Tris-HCl–50 mM NaCl buffer at pH 7.1; relative specific viscosity *vs.* $1/R$; [CT DNA] = 200 μM.

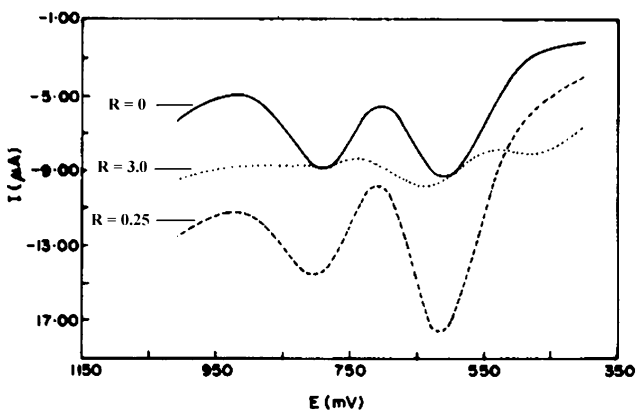

Fig. 10 Differential pulse voltammograms of 0.25 mM $[Ru(Hdpa)_2(dpq)]^{2+}$ **5** in the absence (R = 0) and presence (R = 0.25–3.0) of CT DNA in 5% CH_3OH–5 mM Tris-HCl–50 mM NaCl buffer at pH 7.1 and 25 °C. Scan rate 5 mV s^{-1}; pulse height 50 mV; supporting electrolyte, 50 mM NaCl; working electrode glassy carbon.

obvious that at higher concentrations of DNA the strongly DNA-bound Ru(III) species are immobilized on DNA rendering them incapable of moving to other parts of the biopolymer and effect oxidation of guanine of DNA. Further, the shift in $E_{1/2}$ of **1–4** to a more positive potential (4–70 mV) on binding to DNA reveals that the oxidation of Ru(II) to Ru(III) is rendered difficult. On the other hand, the $E_{1/2}$ of **5** becomes less positive (20 mV) on binding to DNA revealing that the oxidation of Ru(II) to Ru(III) becomes facile. Thus the DNA surface-bound complexes **1** and **2** exhibit guanine oxidation and in fact it has been previously reported that DNA surface-bound complexes such as $[Ru(diimine)_3]^{2+}$ exhibit electrocatalytic oxidation of guanine.[33,57] However, the complexes **3**, **4** and **5** bound to DNA through partial intercalation are involved in electrocatalytic guanine oxidation and it is possible that the partial intercalation of the dpq, mdpq and dppz complexes enables their closer approach to guanine of DNA.

Interaction with supercoiled pBR322 DNA

The interaction of complexes **1–5** with supercoiled pBR322 DNA in 5% CH_3OH–5 mM Tris-HCl–50 mM NaCl buffer at pH 7.1 was studied by agarose gel electrophoresis. The complexes (40 μM) were incubated with DNA (40 μM in base pairs) for 1 h and then subjected to gel electrophoresis. The electrophorogram shows (lanes 2–5, Fig. 11(A)) a pattern for **1–4**, which is very similar to the control indicating that the plasmid DNA is not cleaved. In contrast, the lane 6 for **5** contains no band corresponding to SC or any cleaved NC (form II) or LC form (form III); however, a smearing of DNA is discerned in the gel. When the concentration of **5** is varied from 0 to 100 μM keeping the DNA concentration (40 μM) as constant, the SC form is discernible as a faint band with smearing compared to control

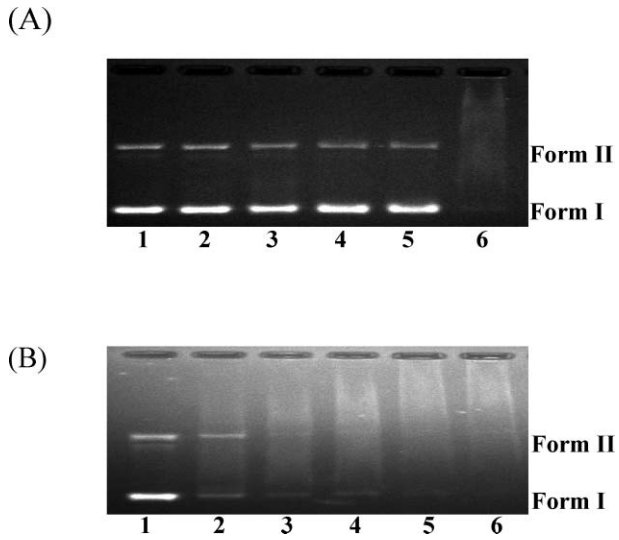

Fig. 11 (A) Gel electrophoresis diagram showing the interaction of complexes **1–5** (40 μM) with supercoiled pBR322 DNA (40 μM in base pair) without added reductant and irradiation in 5% CH_3OH–5 mM Tris-HCl–50 mM NaCl buffer at pH 7.1 and 37 °C with an incubation time of 1 h. lane 1, DNA; lane 2, DNA + **1**; lane 3, DNA + **2**; lane 4, DNA + **3**; lane 5, DNA + **4**; lane 6, DNA + **5**. (B) Various concentrations of **5** were reacted with supercoiled pBR322 plasmid DNA (40 μM in base pair) with an incubation time of 1 h in a 5% CH_3OH–5 mM Tris-HCl–50 mM NaCl buffer at pH 7.1. Lane 1, DNA control; lane 2, DNA + **5** (20 μM); lane 3, DNA + **5** (40 μM); lane 4, DNA + **5** (60 μM); lane 5, DNA + **5** (80 μM); lane 6, DNA + **5** (100 μM). Forms I and II are supercoiled and nicked circular forms of DNA respectively.

at a low complex concentration (20 μM, Fig. 11(B)). At 40–60 μM concentrations of the complex no SC form is detected but, the DNA smear is discerned. At complex concentrations of 80 μM and above DNA smears become faint revealing that EthBr is completely expelled out of the plasmid due to DNA binding of the complex at higher concentrations leading to quenching of EthBr emission (*cf.* above, competitive binding studies). We reason out that the complex molecule **5** intercalates with DNA very strongly and dramatically untwists the plasmid DNA (*cf.* above) leading to structural changes and alteration in the superhelicity[58] of closed circular DNA. Similar inaccessibility of EthBr to plasmid DNA upon addition of $[Ru(bbdo)(dppz)]^{2+}$ has been observed previously.[8] The ability of **1–5** (40 μM) to effect photo-induced DNA strand scission was also examined by incubating them with supercoiled pBR322 DNA (40 μM base pairs) in 5% CH_3OH–5 mM Tris-HCl–50 mM NaCl buffer at pH 7.1 for 1 h. After irradiation with a monochromatic radiation of 365 nm it is found that all the complexes fail to cleave the DNA (result not shown).

Cytotoxicity against cervical epidermoid carcinoma cell line (ME180)

The cytotoxicity of **1–5** against ME180 human cervical epidermoid carcinoma cell line has been investigated in comparison with the widely used drug cisplatin and the structurally analogous and efficient DNA intercalator $[Ru(bpy)_2(dppz)]^{2+}$ under identical conditions by using MTT assay. The observed IC_{50} values (Table 6) reveal that the complexes **1–4** exhibit cytotoxicity lower than cisplatin but higher than $[Ru(bpy)_2(dppz)]^{2+}$ for both 24 and 48 h incubation times. The ability of the complexes to exhibit cytotoxicity follows the order **5** > **3** > **4** > **1** ≅ **2**. Interestingly, the dppz complex **5** exhibits a potency approximately 8 times more than cisplatin for 24 h incubation but 4 times lower activity than cisplatin for 48 h incubation (Table 6). Remarkably, it exhibits approximately 17 and 15 times more potency than the structurally analogous $[Ru(bpy)_2(dppz)]^{2+}$ for 24 and 48 h incubation respectively. The only structural difference between $[Ru(Hdpa)_2(dppz)]^{2+}$ and $[Ru(bpy)_2(dppz)]^{2+}$ is the amine –NH– between two pyridine moieties but its incorporation significantly increases the cytotoxicity of the complex. Thus it is clear that the –NH– group in the primary ligand Hdpa would make significant contributions to the cytotoxicity of the complex. Also, the data on the manual counting of cells with normal and abnormal nuclear features are shown in Fig. 12(A) and it is evident that the number of abnormal cells increases in a time-dependent manner and the complex **5** exhibits a higher percentage of abnormal nuclear features.

Table 6 *In vitro* cytotoxicity assays for complexes **1–5**, cisplatin against cervical epidermoid carcinoma cell line (ME180) (data are mean ±SD of four replicates each). IC_{50} = concentration (mM) of drug required to inhibit growth of 50% of the cancer cells

Complex	IC_{50} (24 h)/μM	IC_{50} (48 h)/μM
$[Ru(Hdpa)_2(phen)]^{2+}$ **1**	30.0 ± 5.0	10.0 ± 2.1
$[Ru(Hdpa)_2(5,6\text{-dmp})]^{2+}$ **2**	15.0 ± 2.5	10.0 ± 1.2
$[Ru(Hdpa)_2(dpq)]^{2+}$ **3**	5.5 ± 1.9	4.25 ± 1.53
$[Ru(Hdpa)_2(mdpq)]^{2+}$ **4**	5.6 ± 1.2	4.8 ± 1.1
$[Ru(Hdpa)_2(dppz)]^{2+}$ **5**	2.50 ± 0.8	2.50 ± 0.9
$[Ru(bpy)_2(dppz)]^{2+}$	42.0 ± 5.5	37.0 ± 3.9
cisplatin	45.74 ± 5.00	1.89 ± 0.06

After treating the cells with IC_{50} concentrations of **5**, which exhibits higher cytotoxicity, for 24 h the cells were observed[2b,31] for cytological changes such as fragmented multinucleation, cell blebbing without micronucleus externalization and cell blebbing with micronucleus externalization adopting Hoechst 33258 staining (Fig. 12(B)). These interesting cytological changes need further investigation to find the mode of cell death.

All the above observations clearly show that the dppz complex **5** exhibits DNA binding affinity higher than the other analogous diimine complexes **1–4**. Also, it is the only complex which alters the DNA superhelicity and causes smearing of the supercoiled pBR322 DNA in the absence of any external reagent or light. We have already shown[8] that $[Ru(N_2S_2)(dppz)]^{2+}$ alters the superhelicity of supercoiled pBR322 DNA, forms DNA-intercalator-EthBr adduct and exhibits a higher cytotoxicity. Further, the complex **5** exhibits a cytotoxicity higher than **1–4**. Similarly, apart from complex **5**, the complex **3** exhibits a higher DNA binding affinity and also a higher cytotoxicity. Finally, the cytotoxicities of the complexes **1–5** are consistent with their abilities to bind with DNA.

Conclusions

Among the mixed ligand complexes $[Ru(Hdpa)_2(diimine)]^{2+}$ the 5,6-dmp complex is involved in hydrophobic interaction while the phen, dpq, mdpq and dppz complexes are involved in intercalation of the diimine ligands into the DNA base pairs. All the DNA binding studies such as absorption, emission and circular dichroic spectral and viscosity experiments suggest that the dppz complex

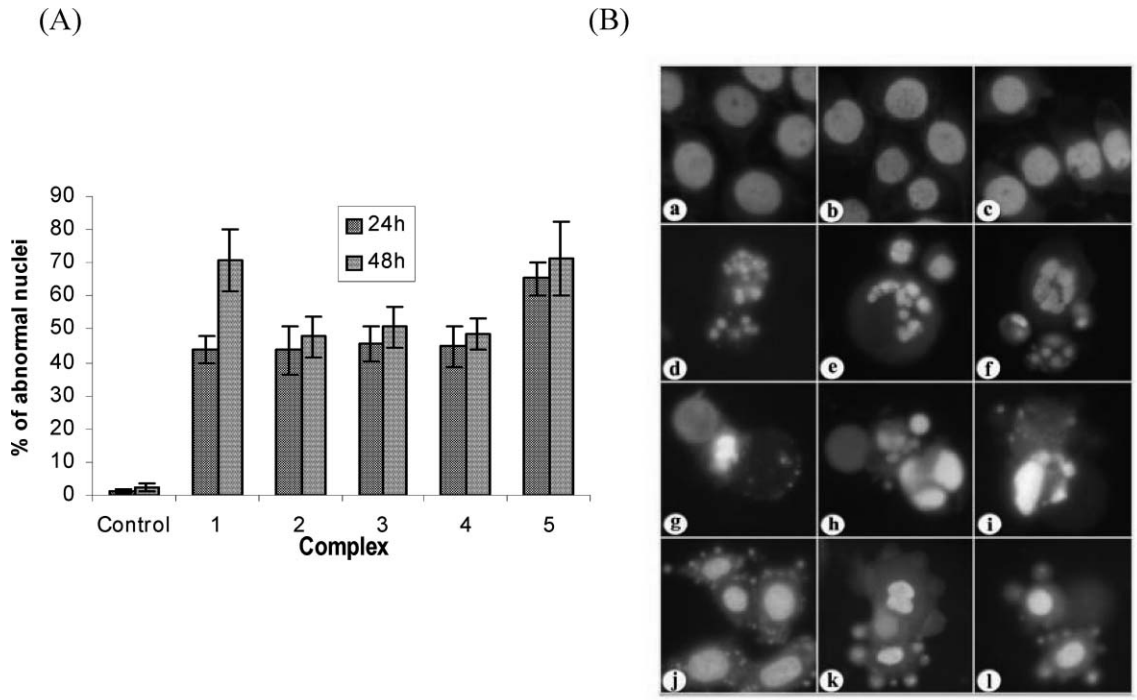

Fig. 12 (A) The percentage of cells in each phase is indicated as a graph. Data are mean values obtained from three independent experiments and bars represent standard deviations. (B) Photomicrograph showing the features of Hoechst 33258 staining of ME180 cervical carcinoma cells: (a–c) untreated cells (control), (d–l) treated with **5**; (d–f) fragmented multinucleation; (g–i) cell blebbing without micronucleus externalization; (j–l) cell blebbing with micronucleus externalization was observed. Cells were treated with **5** after 24 h seeding.

exhibits the highest DNA binding affinity among the present complexes. Interestingly, the complexes **3**, **4** and **5** exhibit ICD and exhibit sequence selectivity by binding more strongly to AT than GC sequence, and the Δ-enantiomers of the *rac*-complexes show the potential to bind preferentially to the right-handed B DNA. In contrast, the 5,6-dmp complex induces a B to Ψ conformational change on CT DNA. Also, all the complexes effect the electrochemical oxidation of guanine moiety of DNA. It is noteworthy that, of all the complexes, the dppz complex alone alters the DNA superhelicity and causes smearing of the supercoiled pBR322 DNA in the absence of any external reagent or light. It is remarkable to find that the same complex exhibits a cytotoxicity higher than the other analogous diimine complexes and also the efficient intercalator $[Ru(bpy)_2(dppz)]^{2+}$ against human cervical epidermoid carcinoma cell line. So it is concluded from this study that both Hdpa as a primary ligand with the H-bonding motif and dppz as an affinity co-ligand have significant potentials as ligand moieties for designing newer metal-based anticancer drugs. We are optimistic that further investigation on the mechanism of action of the dppz compound towards the cell lines would help to rationally design a promising non-covalent and target specific anticancer drug.

Acknowledgements

Council of Scientific and Industrial Research, New Delhi, India (Grant No. 01(2101)/07/EMR-II and SRF to V. R.) is gratefully acknowledged for financial support. Professor M. Palaniandavar is a recipient of Ramanna Fellowship, Department of Science and Technology, New Delhi, India. The Chairman, Molecular Biophysics Unit, Indian Institute of Science, Bangalore is gratefully acknowledged for Circular Dichroism Spectral facility. University Grants Commission (UGC), New Delhi and Department of Science and Technology, New Delhi are gratefully acknowledged for funding to generate Instruments Facility in the Department through Special Assistance Program (SAP) of UGC and Funds for Improvement of S & T Infrastructure (DST-FIST) program of Department of Science and Technology, New Delhi respectively.

References

1 (*a*) M. A. Galindo, D. Olea, M. A. Romero, J. Gomez, P. del Castillo, M. J. Hannon, A. Rodger, F. Zamora and J. A. R. Navarro, *Chem.–Eur. J.*, 2007, **13**, 5075; (*b*) D.-L. Ma, C.-M. Che, F.-M. Siu, M. Yang and K.-Y. Wong, *Inorg. Chem.*, 2007, **46**, 740; (*c*) H.-L. Chan, H.-Q. Liu, B.-C. Tzeng, Y.-S. You, S-M. Peng, M. Yang and C-M. Che, *Inorg. Chem.*, 2002, **41**, 3161.
2 (*a*) B. Rosenberg, L. Van Camp, J. E. Trosko and V. H. Mansour, *Nature*, 1969, **222**, 385; (*b*) E. R. Jamieson and S. J. Lippard, *Chem. Rev.*, 1999, **99**, 2467–2498; (*c*) E. Wong and C. M. Giandomenico, *Chem. Rev.*, 1999, **99**, 2451.
3 *Cisplatin, Chemistry and Biochemistry of a Leading Anti-Cancer Drug*, ed. B. Lippert, Wiley-VCH, Weinheim, 1999, and references therein.
4 I. Meistermann, V. Moreno, M. J. Prieto, E. Molderheim, E. Sletten, S. Khalid, P. M. Rodger and M. J. Hannon, *Proc. Natl. Acad. Sci. USA*, 2002, **99**, 5069.
5 J. Liu, X.-H. Zou, Q.-L. Zhang, W.-J. Mei, J.-Z. Liu and L.-N. Ji, *Met.-Based Drugs*, 2000, **7**, 343.
6 U. Pindur, M. Haber and K. Sattler, *J. Chem. Educ.*, 1993, **70**, 263.
7 (*a*) J. K. Barton, *Science*, 1986, **233**, 727; (*b*) Y. Xiong and L.-N. Ji, *Coord. Chem. Rev.*, 1996, **185**, 711.
8 V. Rajendiran, M. Murali, E. Suresh, S. Shinka, K. Somasundaram and M. Palaniandavar, *Dalton Trans.*, 2008, 148.
9 (*a*) P. B. Dervan and R. W. Burli, *Curr. Opin. Chem. Biol.*, 1999, **3**, 688; (*b*) J.-G. Liu, B.-H. Ye, H. Li, Q.-X. Zhen, L.-N. Ji and Y.-H. Fu, *J. Inorg.*

Biochem., 1999, **76**, 265; (*c*) P. U. Maheswari and M. Palaniandavar, *J. Inorg. Biochem.*, 2004, **98**, 219; (*d*) R. Caspar, L. Musatkina, A. Tatosyan, H. Amouri, M. Gruselle, C. Guyard-Duhayon, R. Duval and C. Cordier, *Inorg. Chem.*, 2004, **43**, 7986.
10 (*a*) A. C. G. Hotze, S. E. Caspers, D. de Vos, H. Kooijman, A. L. Spek, A. Flamigni, M. Bacac, G. Sava, J. G. Haasnoot and J. Reedijk, *J. Biol. Inorg. Chem.*, 2004, **9**, 354; (*b*) A. C. G. Hotze, B. M. Kariuki and M. J. Hannon, *Angew. Chem., Int. Ed.*, 2006, **45**, 4839.
11 (*a*) C. G. Hartinger, S. Zorbas-Seifried, M. A. Jakupec, B. Kynast, H. Zorbas and B. K. Keppler, *J. Inorg. Biochem.*, 2006, **100**, 891; (*b*) M. Galanski, V. B. Arion, M. A. Jakupee and B. K. Keppler, *Curr. Pharm. Des.*, 2003, **9**, 2078; (*c*) M. A. Fuertes, C. Alonso and J. M. Perez, *Chem. Rev.*, 2003, **103**, 645; (*d*) M. J. Clarke, F. C. Zhu and D. R. Frasca, *Chem. Rev.*, 1999, **99**, 2511.
12 M. Cocchietto and G. Sava, *Pharmacol. Toxicol.*, 2000, **87**, 193.
13 (*a*) R. Gagliardi, G. Sava, S. Pacor, G. Mestroni and E. Alessio, *Clin. Exp. Metastasis*, 1994, **12**, 93; (*b*) J. M. Rademaker-Lakhai, D. Van den Bongard, D. Pluim, J. H. Beijnen and J. H. Schellens, *Clin. Cancer Res.*, 2004, **10**, 3717.
14 (*a*) G. Sava, K. Clerici, I. Capozzi, M. Cocchietto, R. Gagliardi, E. Alessio and G. Mestroni, *Anti-Cancer Drugs*, 1999, **10**, 129; (*b*) G. Sava, R. Gagliardi, A. Bergamo, E. Alessio and G. Mestroni, *Anticancer Res.*, 1999, **19**, 969.
15 B. K. Keppler, M. Henn, U. M. Juhl, M. R. Berger, R. Niebl and F. E. Wagner, *Prog. Clin. Biochem. Med.*, 1989, **10**, 41.
16 E. D. Kreuser, B. K. Keppler, W. E. Berdel, A. Piest and E. Thiel, *Semin. Oncol.*, 1992, **19**, 73.
17 (*a*) R. E. Morris, R. E. Aird, P. D. Murdoch, H. M. Chen, J. Cummings, N. D. Hughes, S. Parsons, A. Parkin, G. Boyd, D. I. Jodrell and P. J. Sadler, *J. Med. Chem.*, 2001, **44**, 3616; (*b*) K. Y. Yan, M. Melchart, A. Habtemariam and P. J. Sadler, *Chem. Commun.*, 2005, 4764; (*c*) O. Novakova, H. M. Chen, O. Vrana, A. Rodger, P. J. Sadler and V. Brabec, *Biochemistry*, 2003, **42**, 11544.
18 M. F. Brana, M. Cacho, A. Gradillas, B. de Pascual-Teresa and A. Ramos, *Curr. Pharm. Des.*, 2001, **7**, 1745.
19 R. Cini, S. Defazio, G. Tamasi, M. Casolaro, L. Messori, A. Casini, M. Morpurgo and M. Hursthouse, *Inorg. Chem.*, 2007, **46**, 79.
20 R. E. Shepherd, Y. Chen, R. A. Kortes and M. S. Ward, *Inorg. Chim. Acta*, 2000, **303**, 30.
21 C. Merill, D. Goldman, S. A. Sedman and M. H. Ebert, *Science*, 1980, **211**, 1437.
22 J. G. Collins, A. D. Sleeman, J. R. Aldrich, I. Greguric and T. W. Hambly, *Inorg. Chem.*, 1998, **37**, 3133.
23 C. M. Dupureur and J. K. Barton, *Inorg. Chem.*, 1997, **36**, 33.
24 G. M. Sheldrick, SAINT 5.1, Siemens Industrial Automation Inc., Madison, WI, 1995.
25 SADABS, Empirical Absorption Correction Program, University of Göttingen, Göttingen, Germany, 1997.
26 G. M. Sheldrick, SHELXTL Reference Manual, Version 5.1, Bruker AXS, Madison, WI, 1997.
27 (*a*) G. M. Sheldrick, SHELXS-97: Program for the Solution of Crystal Structures, University of Göttingen, Göttingen, Germany, 1997; (*b*) G. M. Sheldrick, SHELXS-97: Program for the Refinement of Crystal Structures, University of Göttingen, Göttingen, Germany, 1997.
28 *Persistence of Vision Raytracer*, version 3.6; Persistence of Vision Pty. Ltd., Scotland, 1997; http://www.povray.org/download/.
29 J. Bernadou, G. Prativiel, F. Bennis, M. Girardet and B. Meunier, *Biochemistry*, 1989, **28**, 7268.
30 M. Blagosklonny and W. S. El-Diery, *Int. J. Cancer*, 1996, **67**, 386.
31 G. P. A. H. Kasibhatla D. Finucane, T. Brunner, E. B. Wetzel and D. R. Green, Protocol: Staining of Suspension Cells with Hoechst 33258 to Detect Apoptosis, *Cell: A Laboratory Manual: Culture and Biochemical Analysis of Cells*, 2000, vol. 1, pp. 15.5, CSHL Press, USA, 1998.
32 M. Murali and M. Palaniandavar, *Dalton Trans.*, 2006, 730.
33 P. A. Anderson, G. B. Deacon, K. H. Haarmann, F. R. Keene, T. J. Meyer, D. A. Reitsma, B. W. Skelton, G. F. Strouse, N. C. Thomas, J. A. Treadway and A. H. White, *Inorg. Chem.*, 1995, **34**, 6145.
34 P. U. Maheswari, V. Rajendiran, H. S. Evans and M. Planiandavar, *Inorg. Chem.*, 2006, **45**, 37.
35 P. J. Steel, F. Lahousse, D. Lerner and C. Marzin, *Inorg. Chem.*, 1983, **22**, 1488.
36 (*a*) P. U. Maheswari, V. Rajendiran, M. Palaniandavar, R. Thomas and G. U. Kulkarni, *Inorg. Chim. Acta*, 2006, **359**, 4601; (*b*) J. G. Collins, A. D. Sleeman, J. R. Aldrich-Wright, I. Greguric and T. W. Hambley, *Inorg. Chem.*, 1998, **37**, 3133.
37 N. Nagao, M. Mukaida, S. Tachiyashiki and K. Mizumachi, *Bull. Chem. Soc. Jpn.*, 1994, **67**, 1802.
38 D. P. Segers and M. K. DeArmond, *J. Phys. Chem.*, 1982, **86**, 3768.
39 R. L. Blakley and M. K. DeArmond, *J. Am. Chem. Soc.*, 1987, **109**, 4895.
40 S. P. Foxon, C. Metcalfe, H. Adams, M. Webb and J. A. Thomas, *Inorg. Chem.*, 2007, **46**, 409.
41 A. M. Pyle, J. P. Rehmann, R. Meshoyrer, C. V. Kumar, N. J. Turro and J. K. Barton, *J. Am. Chem. Soc.*, 1989, **111**, 3051.
42 M. Lee, A. L. Rhodes, M. D. Wyatt, S. Forrow and J. A. Hartley, *Biochemistry*, 1993, **32**, 4237.
43 R. B. Lopez, B. L. Loen, T. Boussie and T. J. Meyer, *Tetrahedron Lett.*, 1996, **37**, 5437.
44 B. Selvakumar, V. Rajendiran, P. U. Maheswari, H. S. Evans and M. Palaniandavar, *J. Inorg. Biochem.*, 2006, **100**, 316.
45 V. I. Ivanov, L. E. Minchenkova, A. K. Schyolkina and A. I. Poletayer, *Biopolymers*, 1973, **12**, 89.
46 P. Lincoln, E. Tuite and B. Norden, *J. Am. Chem. Soc.*, 1997, **119**, 1454.
47 B. Norden and F. Tjerneld, *Biopolymers*, 1982, **21**, 1713.
48 S. Delaney, M. Pascaly, P. Bhattarcharya, K. Han and J. K. Barton, *Inorg. Chem.*, 2002, **41**, 1966.
49 C. Hiort, B. Norden and A. Rodger, *J. Am. Chem. Soc.*, 1990, **112**, 1971.
50 G. A. Mines, J. A. Roberts and J. T. Hupp, *Inorg. Chem.*, 1992, **31**, 125.
51 B. I. Kankia, V. Buckin and V. A. Bloomfield, *Nucleic Acids Res.*, 2001, **29**, 2795.
52 L. S. Lerman, *J. Mol. Biol.*, 1961, **3**, 18.
53 M. J. Warning, *J. Mol. Biol.*, 1970, **54**, 247.
54 D. E. Morris, Y. Ohsawa, P. Segers, K. Dearmond and K. W. Hanck, *Inorg. Chem.*, 1984, **23**, 3010.
55 D. E. Morris, K. W. Hanckand and M. K. Dearmond, *Inorg. Chem.*, 1985, **24**, 977.
56 S. Mahadevan and M. Palaniandavar, *Bioconjugate Chem.*, 1996, **7**, 138.
57 T. W. Welch, A. H. Corbett and H. H. Thorp, *J. Phys. Chem.*, 1995, **99**, 11757.
58 E. C. Long and J. K. Barton, *Acc. Chem. Res.*, 1990, **23**, 271.

